Minimal Model of Plasma Membrane Heterogeneity Requires Coupling Cortical Actin to Criticality

Benjamin B. Machta,[†] Stefanos Papanikolaou,[†] James P. Sethna,[†] and Sarah L. Veatch[‡]

[†]Department of Physics and [‡]Department of Chemistry and Chemical Biology, Cornell University, Ithaca, New York

Supplementary Information

1. Introduction:

Sections 1-4 of this supplement serve to give more complete details of the methods used in the simulations. Sections 5-8 discuss theoretical details which underlie our choice of model, discussing in more detail its benefits and limitations. In sections 2 and 3 we discuss the construction of figure 1. In section 4 we describe our simulations in sufficient detail that a reader could reproduce figures 2-5 in the main text. In section 5 we explain why we may, without significant effect, neglect the tilt of the rectilinear diameter in figure 1A of the main text. In section 6 we give arguments justifying our use of the Ising model to describe cell plasma membranes. In section 7, we justify our use of 'model B', Kawasaki dynamics. In section 8 we discuss how our results depend on the relative viscosities in the two phases.

2. Calculation of Correlation Length Contours in Figure 1A:

Following Combescot et al. [1] the correlation length as a function of thermodynamic parameters has a simple form in a sort of 'polar' coordinates[2-3]. A coordinate transformation takes these to the more familiar axes of reduced temperature and magnetization. We change coordinates a second time by introducing a non-zero arbitrary tilt, allowing for a non-universal correction which arises if a change in real temperature in a membrane corresponds to a change in both reduced temperature and magnetization in the Ising model. In the critical region this tilt is captured in a single parameter, continuous through the critical point, called the slope of the *rectilinear diameter* [4], which is non-universal and so may be different for different systems in the same universality class. Though it has not been quantified, in GPMVs it is within

experimental bounds of zero as can be seen in the supplemental videos of [5]. It could theoretically be measured by looking at the change in the surface area of bright to dark regions as temperature is lowered below the critical point. Though experiments cannot differentiate the true tilt from zero, we include a small tilt here of 0.1 to stress that we do not expect it to be exactly zero. The contours all multiply a non-universal 'natural length scale' which is taken from experiments in plasma membrane vesicles [5]. Finally, we note that GPMVs in [5] have a spread in their critical temperatures of around 10°C, which corresponds to a spread in their reduced temperatures at 37°C of about .03. Though it has not been quantified, we expect there is also some spread in their effective magnetizations. Together, we expect that there is some variation from cell to cell both vertically and horizontally in the exact placement of the red dot corresponding to physiological conditions. We choose an average value of T_c=22°C at critical composition for this figure and most of the results in the paper. Ignoring a possible deviation in the magnetization is justified in section 5 below.

3. Preparation of cell attached plasma membrane vesicles in figure 1B:

Cell attached plasma membrane vesicles are prepared as described previously [5-6]. Briefly, RBL-2H3 mast cells are plated sparsely in a MatTek well (MatTek Corp. Ashland, MA) overnight. Cells are then incubated for 1h at 37°C in the presence of active bleb buffer (2 mM $CaCl_2$ /10 mM Hepes/0.15 M NaCl, 25 mM HCHO, 2 mM DTT, pH 7.4). Cells and attached vesicles are then labeled with DiIC12 (Invitrogen.Eugine, OR) dissolved in methanol for 5min prior to viewing on an inverted microscope (DM-IRB; Leica Microsystems, Bannockburn, IL) at room temperature. The image was taken using an EMCCD camera (iXon 897; Andor, Belfast U.K.). Under these conditions, attached blebs contain coexisting liquid-disordered (bright) and liquid-ordered (dark) phases.

4. Simulation details, acceptance criterion and equilibration procedures:

All simulations were run on a 400x400 bi-periodic square lattice with spin variables living on the squares (S_i=±1, white and black pixels respectively). In all cases

the standard Ising Hamiltonian is used, given by $H = -\sum_{\{i,j\}} S_i S_j$ with summation over the four nearest neighbors. We use a conversion factor from lattice constant to real distance of 1nm. Temperatures are converted to Kelvin (and by extension Celsius) by equating the exact critical temperature given by the Onsager solution on the square lattice, $T_c = \frac{2}{\log(1+\sqrt{2})}$ with 295K so that $T_{sim} = 0.00769 T_{real}$, where T_{real} is in Kelvin. In a Monte-Carlo 'sweep' 160,000 (400^2) pairs of pixels are proposed (on average each pixel is proposed to exchange twice). We use Metropolis spin exchanges; each pair is exchanged or not so as to satisfy detailed balance[7]. If the resulting configuration is lower in energy, the exchange is always accepted. If the energy is raised, the exchange is accepted stochastically with probability $\exp(-\beta \Delta H)$ where β is the inverse temperature and ΔH is the change in energy between initial and final states. Sites occupied by pickets are taken to have an infinite field so that exchanges which propose to move a black pixel onto a picket are always rejected. Where appropriate, 'strongly coupled' tracers have an infinite coupling to other like pixels, so that any move which ends with such a strongly coupled tracer touching an unlike pixel is always rejected. This effectively converts them into cross shaped objects (though with overlap allowed), with three times as many bonds to their local environment and twice as many neighbors.

Two types of dynamics are employed (any dynamics which satisfy detailed balance will lead to the same equilibrium ensemble of configurations). When rapid equilibration is desired we employ nonlocal moves where each of a pairs of spins are randomly chosen from all sites on the lattice. To simulate real time we use Kawasaki dynamics where we randomly choose a spin, and then randomly choose one of its four nearest neighbors to exchange with.

Equilibration is very rapid using the nonlocal dynamics, where z is near 2. We always equilibrate for 100,000 sweeps using nonlocal moves starting from a distribution which observes the random field constraint but which is otherwise random. 100,000 sweeps is many times longer than the decay time of the slowest decaying system used here (the decay time is around 1000 sweeps for the pinning density in Fig. 2-4 at $1.05T_c$.

as can be seen by eye looking at snapshots at subsequent times, or quantitatively as the decay time of time-time correlations). For simulations with strong tracers we first equilibrate without tracers. We then add them randomly, run an additional 100,000 iterations to equilibrate, and then start our dynamic simulations.

In figure 2 no dynamics are required as only a snapshot is given. In figure 3, the time averaged spatial correlation figures are averaged from 1000 snapshots each separated by 1000 sweeps of the non-local dynamics. The auto-correlation functions in figure 3 are produced in the standard way. We first Fourier transform the spin configuration. We then square this to get the static structure factor S(k). We then perform an inverse Fourier transform on S(k) and radially average the result to get g(r) in a normalization which goes to 0 at infinity. To convert to the normalization used here, $G(r) = \frac{< P_{+1}(R)P_{+1}(R+r) >}{< P_{+1}(R)P_{+1}(\infty) >}$ (where R is averaged over the entire lattice and where $P_{+1}(x)$ is the probability of an up spin at position x) we add one to these (since all of our correlation functions are plotted at m=0). We assume that the lattice sits on an infinite periodic plane so that values at ∞ take the mean value of the system.

To produce the cross-correlation curves we follow the same procedure except that we replace the square of the Fourier transform with the real part of the product of the Fourier transform of the pixel configuration and the Fourier transform of the random field configuration. This leads to $G(r) = \frac{< Pcyt(R)P_{+1}(R+r) >}{< Pcyt(R)P_{+1}(\infty) >}$ where $P_{cyt}(x)$ is the probability of finding a cytoskeletal pixel at position x.

For time-time correlations shown in Fig 4a we take the dot product of every pixel in the simulation's value (± 1) at time t with itself at a later time $t+\Delta t$. We average this over all pixels and all times $t<t_{max}-\Delta t$, with t_{max}=5,000,000 sweeps and add one to the value for consistency with our normalization (in supplemental fig S1 two different realizations of this procedure are shown to give the reader an idea of the expected error). To produce the dashed lines which correspond to the asymptotic values of the correlation functions in the presence of the random field we take the average value of the square of the mean field pixel values from the configuration calculated from the non-local

dynamics (which are identical and faster to equilibrate, displayed in Fig3A,C) and add one to this value.

To convert from Monte-Carlo time to real time, we use a microscopic diffusion constant of $1\mu m^2/s$ which is in the middle of the range cited for membrane bound lipids and proteins (though this range spans some 2 orders of magnitude)[8-10]. In a Monte-Carlo sweep, each pixel is proposed to swap twice on average. If all swaps were accepted this would lead to a mean squared displacement $\langle x^2 \rangle = 2\, d^2$/sweep where d is the lattice spacing. With our value of d=1nm, we find that if we associate one sweep with .5μs we arrive at the desired $D=1\mu m^2/s$ in the formula for diffusion $\langle x^2 \rangle = 4Dt$. As some moves are rejected, the effective diffusion constant even at arbitrarily short times is actually somewhat lower than this for traced diffusing pixels and slower still for our more strongly coupled diffusers.

To calculate mean squared displacements we trace 1000 particles which diffuse on an infinite plane whose configuration is periodic with period 400. Whenever a particle moves through a boundary in the ± x direction (for example), its new position for the purpose of mean squared displacement calculation is changed by ±400. This allows us to keep track of tracers which may diffuse off of the edge of the periodic simulation. We average the mean squared displacements over all traced particles.

To produce the contour plots in fig 5 we extrapolate and smooth between the points where simulations are conducted by replacing each point's value by an average over all simulated points weighted by $\exp(-d^2 / d_0^2)$ where $d_0 = .1$ in temperature, pinning density and magnetization.

5. Irrelevance of a tilted rectilinear diameter to lowest order:

As discussed in 'Calculation of correlation length contours' a change in real temperature near a critical point changes both of the corresponding Ising variables of reduced temperature and magnetization. Here we show that such a tilt introduces a subdominant correction to the critical properties. In particular it does not affect the singular behavior of the correlation length

In the scaling regime, a temperature change corresponds to a change in the reduced temperature by an amount Δt and a change in the magnetization by an amount $\Delta m = a\Delta t$ where a is the tilt of the rectilinear diameter[4]. We here consider a model in the scaling regime whose correlation length is given by $\xi(t,m) = t^{-\nu} F(m^{\nu/\beta}/t)$ where F is a universal function. We note that F is not singular at zero, since along the $m = 0$ axis the correct scaling is given by $\xi(t,0) \sim t^{-\nu}$. We now set $m = at$ which corresponds to a membrane with critical composition taken to a temperature $T = (1+t)T_c$. This gives $\xi(t,m) = \xi(t,at) = t^{-\nu} F(a^{\nu/\beta} t^{\nu/\beta - 1})$. Because $\nu/\beta = 8 > 1$, the argument of F is not singular near t=0. As F itself is not singular there, the scaling of the correlation length $\xi(t,m)$ at critical composition has singular behavior $\xi(t,0) \sim t^{-\nu}$ which is independent of the tilt of the rectilinear diameter. (In addition to the "analytic correction to scaling" represented by the tilting of the rectilinear diameter proportional to $T_c - T$, there is also a singular correction to scaling proportional to $(T_c - T)^{1-\alpha}$. Since $\alpha=0$ for the 2D Ising model, our argument above applies without modification; this correction too is subdominant. See [3] , [11-12] and for details, and a more complete picture of subtleties involved.) This means that the critical properties of an Ising system at critical composition but slightly away from the critical temperature are dominated by its effective reduced temperature, with its effective magnetization coming in only at a higher order in the distance from the critical point. This calculation quantifies what can be seen in Fig 1A of the paper; Near the critical point the contours are broad and flat showing a larger dependence on the vertical 'reduced temperature' direction than on the horizontal 'magnetization' direction.

6. Possible universality classes:

Here we give arguments to support our use of the 2-D Ising universality class to model the critical point seen in GPMVs [5]. We explain the theoretical motivation for expecting Ising criticality, discuss experimental evidence for it and argue that two other possible universality classes are unlikely to describe cellular membranes.

The Ising Universality class is expected for any system with a *scalar order parameter*, a single number which describes the system at larger length scales. In three dimensions, the Ising model has been shown to quantitatively describe an enormous array of liquid-gas and liquid-liquid critical points [3] mostly involving small molecules, but also including more exotic liquid phases containing polymer blends [13]. In two dimensions there are fewer examples, but the critical phenomenon seen in three component model membranes near fluid-fluid critical points are in this class [14]. In each of these two and three dimensional examples the components (or densities) of the two low temperature phases acts as the order parameter, which is therefore a scalar. Plasma membrane vesicles are certainly more complicated than the simple systems described above at the microscopic level, but as they phase separate into two domains with different compositions below T_c, the composition difference between these phases remains a good scalar order parameter. As such, the theoretical expectation is that they should also be described by 2-D Ising Universality, which is in agreement with [5].

We cannot exhaustively dismiss other possible universality classes at present, though several cases can be ruled out. The q-state Potts universality class generalizes the Ising model (q=2) to the critical point of a system which separates into q distinct liquids below T_c [15]. For q=3 and 4 there are 2-D critical points, while for q larger, there are only abrupt, first order transitions. These models are ruled out quite simply by the GPMV experiments. The q-state Potts model predicts that below T_c a Potts critical membrane should phase separate into q domains of approximately equal area. To our knowledge no more than two coexisting macroscopic liquid phases have been observed in any membrane system. We note as an aside that Potts models with q>2 would be dramatically harder for a cell to tune towards. The Ising critical point contains two parameters which must be tuned. At fixed temperature we must tune the ratio of the two phases below T_c and their interaction energies. The 3-state Potts model contains five parameters that need tuning [15]. We can think of these as two area ratios (A:B and B:C) as well as three interaction energies (A with B, B with C and A with C).

Another possibility is that the membrane might display tri-critical Ising behavior. This occurs as an Ising model is tuned (along a third dimension in parameter space) to a

boundary beyond which it becomes an abrupt first order transition. This model would only require tuning one additional parameter making it at first pass more appealing. However, it predicts a value for the critical exponent of $\nu=5/9$ [15], in contrast to $\nu=1$ for the Ising model, which is not consistent with existing experimental data [5].

Although we are not able to conclusively demonstrate that the universality class is Ising at this time, we emphasize that our results should hold even if the universality class turns out to be more exotic. The qualitative features of our findings come about due to features which have been conclusively demonstrated in GPMV experiments [5]: A correlation length which becomes large near the critical point, and dynamics which become slow near the critical point. Although it is outside of the scope of this work, we also note that there has been significant theoretical progress towards a complete categorization of possible universality classes permissible in 2-D [15]. Though there are infinitely many, they are all indexed by a unique number between zero and one, the central charge (which is 0.5 for the Ising model). It would be an interesting project to see which if any others might be consistent with membrane experiments.

7. Dynamic universality and motivation for model B:

The Ising universality class defines the coarse grained static correlation functions of our system. However, different systems in the same universality class can display different dynamics even in the scaling regime. These in turn fall into different dynamic scaling universality classes[16] which are determined by which quantities are conserved by the dynamics. In our case, we argue that the order parameter (or composition) is locally conserved, while momentum is not, as the fixed cytoskeleton breaks translational invariance, and may exchange momentum with the membrane. With the order parameter conserved and momentum not, we expect model B[16]. The Kawasaki dynamics we implement here are also in this class[17].

Membranes are expected to have a conserved order parameter for the times relevant to this study. The two low temperature phases contain different concentrations of various components. For a region's order parameter to change, components must physically move into it from a neighboring region. Although components are found with

some probability in each low temperature phase (and are able to move between them), this is not qualitatively different from the Ising model where white pixels and even white pixel clusters are found in the low temperature black pixel phase. At longer times we expect processes like trafficking of lipids to change the order parameter[18].

We also expect that in intact cell plasma membranes momentum will not be conserved at relevant lengths, leading to model B (rather than model H, which arises when momentum is also conserved). There is an emerging theoretical picture for the expected dynamics of model membranes near an Ising critical point, immersed in water. In two dimensions the usual Stokes-Einstein relations which predict the microscopic diffusion constant as a function of the diffuser's size and the viscosity of the surrounding fluid cannot be easily applied [19] essentially because energy is not locally dissipated. For large inclusions this means that even an arbitrarily small viscosity of the surrounding fluid enters into the microscopic diffusion rate. It also means that this diffusion constant depends only logarithmically on the size of the diffuser, crossing over to a rate determined by the 3-D viscosity (which scales as 1/r) for large enough r [20]. For lipids in a bilayer membrane, the picture is somewhat simpler. Such lipids show an enormous temperature dependence in their microscopic diffusion rates [10] consistent with an energy barrier of 20-30 K_BT. These rates are approximately two orders of magnitude faster than the rates predicted by the hydrodynamic diffusion constant extrapolated from the movement of micron sized diffusers [20] in similar liquid environments. This suggests the following picture [21]: rather than their motion being dominated by hydrodynamic flow, lipids sit in deep potential wells in the membrane. Their microscopic diffusion rate is set by the likelihood of thermally hopping into the next potential well – model B, rather than model H, governs the particle diffusion rate. Thus membranes are similar to liquids above the glass transition, where self-diffusion (mediated by swapping particles) is much faster than bulk diffusion. (In a crystal, the latter would be zero.)

Even though particle diffusion is dominated by model B, we must address also the evolution of the order parameter field. Hydrodynamic flows are more effective at "stirring" the order parameter field than particle exchanges. This is reflected in the

dynamical critical exponent z, which is 3.75 for model B and around 2 for model H in two dimensions [16, 22]. Roughly, correlation times at a length-scale L scale as $(L/L_0)^z$ (critical slowing-down). Since at the lipid length scale of one nm the time scales for hopping and hydrodynamic rates differ by two orders of magnitude, this suggests that the hydrodynamic effects will become competitive with the model B dynamics at roughly 10nm (where $D_{lipid}(L/L_0)^{3.75} \sim D_{hydro}(L/L_0)^2$), which is roughly the equilibrium correlation length where both power laws stop applying. In the absence of a cytoskeleton and at the critical temperature, the hydrodynamic diffusion will dominate in a range of lengths between this crossover and a crossover to a modified three-dimensional model H dynamics (when the low viscosity of the surrounding water becomes relevant, at around 1000nm) [22]. The rigid cytoskeleton will act as a fixed boundary condition at a significantly shorter length scale in our model, suppressing hydrodynamic flows entirely while permeable to hopping diffusion. (The cytoskeleton should be particularly effective at suppressing the logarithmic correlations in the 2D hydrodynamics.) Hence our model B dynamics not only dominates the diffusion of small particles, it also should dominate the dynamics of the order parameter field except for small corrections in a range intermediate between the correlation length and the cytoskeleton confinement scale. We finally note that coupling to a cytoplasm with many rigid objects nearby may lead to even more suppression of bulk flow in the membrane as discussed in [23]

8. Effects of different viscosities in the two liquid environments:

The l_0 and l_d phases represented by our white and black pixels have viscosities which differ by a factor of around 4 though in some cases up to a factor of 10 [9-10, 24]. A similar range is expected in the diffusion constant difference seen between lipids in the two phases. In most of the manuscript we ignore the consequences of this, but we discuss its implications here. The dynamics of the order parameter are relatively unaffected by this as order parameter changes always take place at the interface and so have a single rate which is presumably somewhere in between the rates predicted by the individual viscosities.

Traced particle diffusion, however, can be affected by this viscosity difference. We consider the case relevant to our dynamics; a particle which mostly resides in one of the two phases, but which may need to cross through the other phase to diffuse long distances. The microscopic diffusion constant will be an average of the diffusion constants in the two phases weighted by the time spent in each phase. For us it will be given primarily by the diffusion constant in the phase in which it usually resides.

To travel large distances these particles potentially needs to hop over barriers of the alternative phase, which leads to the confinement seen in our simulations. We separate this process into an attempt rate at crossing and a success probability. The total amount of time spent in the unfavorable region, as well as the success probability are determined by static energetic considerations; they does not depend on the relative viscosities. The attempt rate, however, must depend on the ratio of the diffusion constants in the two liquids. In particular, to satisfy detailed balance it must go as the ratio of the viscosity in the usual fluid environment to that in the barrier environment. As such, particles which mostly live in the low viscosity environment make fewer attempts at crossing the barrier, while those which live mostly in the higher viscosity environment make more. This can lead to some additional confinement for particles which live in the lower viscosity phase. The extra confinement is bounded by the ratio of the two viscosities.

To demonstrate these theoretical predictions we run simulations where the diffusion rates in the two liquid environments are different by a factor of four, mimicking a factor of four change in the viscosity. We implement this by trading like particles in the lower viscosity liquid with a rate four times that with which unlike particles and particles in the high viscosity liquid are traded. We run simulations where either the white pixels or the black ones have a higher viscosity. We then plot MSDs vs time (fig S2), for the cases where both liquids are equivalent, and where the given particle is either a component of the lower or higher viscosity liquid. In each case the y-axis is normalized to 1 at t=1ms (in the equal viscosity case), and we compress the x-axis for the high viscosity case so that the frequency of moves per unit ‘time’ on the x-axis is the same. We also plot a dashed line corresponding to a lack of any confinement. We note that in

our simulations this consequences of this effect are fairly small.

References

1. **Combescot, M., M. Droz, and J.M. Kosterlitz, *Two point correlation function for general fields and temperatures in the critical region.* Physical Review B, 1975. 11(Copyright (C) 2010 The American Physical Society): p. 4661.**
2. **Schofiel.P, *Parametric Representation of Equation of State near a Critical Point.* Physical Review Letters, 1969. 22(12): p. 606-&.**
3. **Sethna, J.P., *Statistical mechanics : entropy, order parameters, and complexity*. Oxford master series in statistical, computational, and theoretical physics. 2006, Oxford ; New York: Oxford University Press. xix, 349 p.**
4. **Zollweg, J.A. and Mulholla.Gw, *Law of Rectilinear Diameter.* Journal of Chemical Physics, 1972. 57(3): p. 1021-&.**
5. **Veatch, S.L., et al., *Critical fluctuations in plasma membrane vesicles.* ACS Chem Biol, 2008. 3(5): p. 287-93.**
6. **Baumgart, T., et al., *Large-scale fluid/fluid phase separation of proteins and lipids in giant plasma membrane vesicles.* Proc Natl Acad Sci U S A, 2007. 104(9): p. 3165-70.**
7. **Newman, M.E.J. and G.T. Barkema, *Monte Carlo methods in statistical physics*. 1999, Oxford New York: Clarendon Press ;**
Oxford University Press. xiv, 475 p.
8. **Eggeling, C., et al., *Direct observation of the nanoscale dynamics of membrane lipids in a living cell.* Nature, 2009. 457(7233): p. 1159-U121.**
9. **Lingwood, D., et al., *Plasma membranes are poised for activation of raft phase coalescence at physiological temperature.* Proceedings of the National Academy of Sciences of the United States of America, 2008. 105(29): p. 10005-10010.**
10. **Filippov, A., G. Oradd, and G. Lindblom, *The effect of cholesterol on the lateral diffusion of phospholipids in oriented bilayers.* Biophysical Journal, 2003. 84(5): p. 3079-86.**
11. **Goldstein, R.E. and N.W. Ashcroft, *ORIGIN OF THE SINGULAR DIAMETER IN THE COEXISTENCE CURVE OF A METAL.* Physical Review Letters, 1985. 55(20): p. 2164-2167.**
12. **Wang, J., et al., *Principle of isomorphism and complete scaling for binary-fluid criticality.* Phys Rev E Stat Nonlin Soft Matter Phys, 2008. 77(3 Pt 1): p. 031127.**
13. **Schwahn, D., K. Mortensen, and H. Yee-Madeira, *Mean-field and Ising critical behavior of a polymer blend.* Phys Rev Lett, 1987. 58(15): p. 1544-1546.**
14. **Honerkamp-Smith, A.R., et al., *Line tensions, correlation lengths, and critical exponents in lipid membranes near critical points.* Biophysical Journal, 2008. 95(1): p. 236-46.**
15. **Di Francesco, P., P. Mathieu, and D. Sénéchal, *Conformal field theory*. Graduate texts in contemporary physics. 1997, New York: Springer. xxi, 890 p.**
16. **Hohenberg, P.C. and B.I. Halperin, *THEORY OF DYNAMIC CRITICAL PHENOMENA.* Reviews of Modern Physics, 1977. 49(3): p. 435-479.**
17. **Yalabik, M.C. and J.D. Gunton, *MONTE-CARLO RENORMALIZATION-GROUP STUDIES OF KINETIC ISING-MODELS.* Physical Review B, 1982. 25(1): p. 534-537.**
18. **Fan, J., M. Sammalkorpi, and M. Haataja, *Domain formation in the plasma membrane: Roles of nonequilibrium lipid transport and membrane proteins.* Physical Review Letters, 2008. 100(17): p. -.**
19. **Saffman, P.G. and M. Delbruck, *Brownian motion in biological membranes.* Proc Natl Acad Sci U S A, 1975. 72(8): p. 3111-3.**

20. **Cicuta, P., S.L. Keller, and S.L. Veatch,** ***Diffusion of liquid domains in lipid bilayer membranes.*** **J Phys Chem B, 2007. 111(13): p. 3328-31.**

21. **Vaz, W.L.C., R.M. Clegg, and D. Hallmann,** ***Translational Diffusion of Lipids in Liquid-Crystalline Phase Phosphatidylcholine Multibilayers - a Comparison of Experiment with Theory.*** **Biochemistry, 1985. 24(3): p. 781-786.**

22. **Haataja, M.,** ***Critical dynamics in multicomponent lipid membranes.*** **Phys Rev E Stat Nonlin Soft Matter Phys, 2009. 80(2 Pt 1): p. 020902.**

23. **Tserkovnyak, Y. and D.R. Nelson,** ***Conditions for extreme sensitivity of protein diffusion in membranes to cell environments.*** **Proc Natl Acad Sci U S A, 2006. 103(41): p. 15002-7.**

24. **Kahya, N., et al.,** ***Probing lipid mobility of raft-exhibiting model membranes by fluorescence correlation spectroscopy.*** **Journal of Biological Chemistry, 2003. 278(30): p. 28109-28115.**

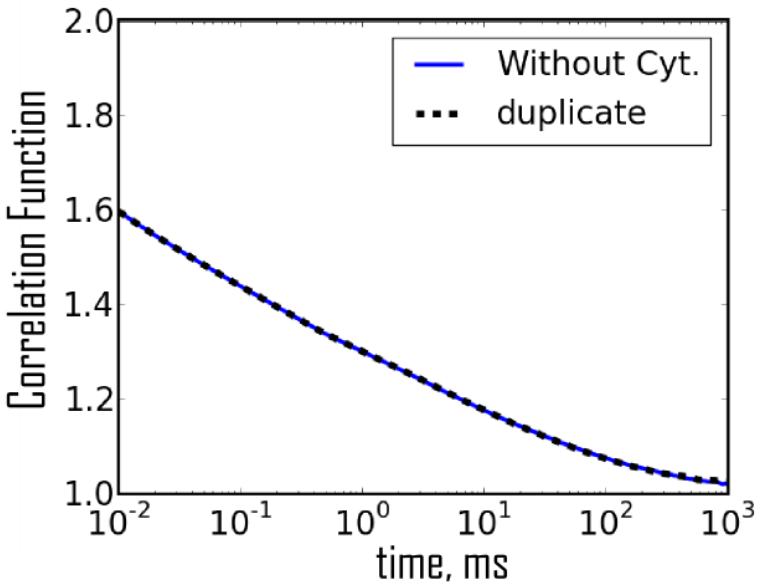

Figure S1 To demonstrate the accuracy of our time-time correlation functions, we reproduce the slowest decaying curve from the fig. 4A and plot both versions on the same graph. A slight deviation is visible at very late times.

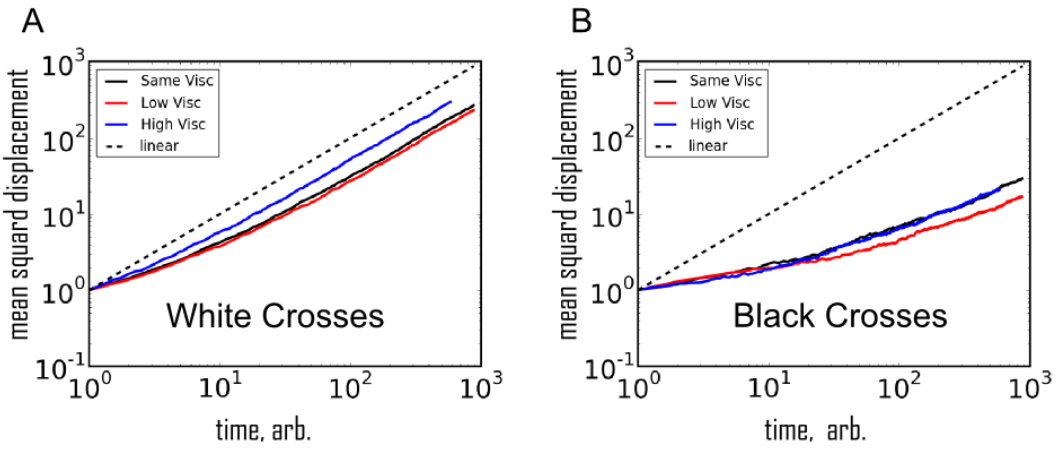

Figure S2 The mean squared displacement of strongly coupled white (A) and black (B) diffusers at 1.05T_c,with the same static properties as in Fig 4 D of the main text. In each figure the black line shows the mean square displacement for the case when both viscosities are equal. In the other cases the diffuser is a component of the high (blue) or low (red) viscosity liquid. The y-axis is normalized to 1 at a time such that the traced particle has performed on average 2000 attempted exchanges. The x-axis is normalized so that in each case the displayed traced particles are proposed to swap approximately 2000 times (0.5 ms in the main text) so that all have an identical microscopic attempt rate. As can be seen, particles that normally inhabit the low viscosity liquid see some degree of extra confinement, and vice versa.